RSC Advances

PAPER

View Article Online
View Journal | View Issue

Cite this: *RSC Adv.*, 2020, **10**, 7012

Ginkgo biloba leaf polysaccharide stabilized palladium nanoparticles with enhanced peroxidase-like property for the colorimetric detection of glucose†

Yanshuai Cui,[a] Xiang Lai,[b] Kai Liu,[b] Bo Liang,*[a] Guanglong Ma[c] and Longgang Wang[b]

Sensitive glucose detection based on nanoparticles is good for the prevention of illness in our bodies. However, many nanoparticles lack stability and biocompatibility, which restrict their sensitivity to glucose detection. Herein, stable and biocompatible *Ginkgo biloba* leaf polysaccharide (GBLP) stabilized palladium nanoparticles (Pd_n-GBLP NPs) were prepared through a green method where GBLP was used as a reducing and stabilizing agent. The results of Pd_n-GBLP NPs characterized by UV-visible spectroscopy (UV-Vis), Fourier transform infrared (FTIR) spectroscopy, transmission electron microscopy (TEM) and X-ray photoelectron spectra (XPS) confirmed the successful preparation of Pd_n-GBLP NPs. TEM results indicated that the sizes of Pd NPs inside of Pd_n-GBLP NPs (n = 41, 68, 91 and 137) were 7.61, 9.62, 11.10 and 13.13 nm, respectively. XPS confirmed the successful reduction of $PdCl_4^{2-}$ into Pd (0). Dynamic light scattering (DLS) results demonstrated the long-term stability of Pd_n-GBLP NPs in different buffer solutions. Furthermore, Pd_{91}-GBLP NPs were highly biocompatible after incubation (500 μg mL^{-1}) with HeLa cells for 24 h. More importantly, Pd_{91}-GBLP NPs had peroxidase-like properties and followed a ping-pong mechanism. The catalytic oxidation of substrate 3,3′,5,5′-tetramethylbenzidine (TMB) into blue oxidized TMB (oxTMB) by Pd_{91}-GBLP NPs was used to detect the glucose concentration. This colorimetric method had high selectivity, wide linear range from 2.5 to 700 μM and a low detection limit of 1 μM. This method also showed good accuracy for the detection of glucose concentrations in blood. The established method has great potential in biomedical detection in the future.

Received 22nd January 2020
Accepted 10th February 2020

DOI: 10.1039/d0ra00680g

rsc.li/rsc-advances

1. Introduction

Natural enzymes have excellent catalytic activity and specificity for substrates leading to broad applications in bio-related detection. These natural enzymes include L-glutamic acid decarboxylase, horseradish peroxidase (HRP), alkaline phosphatase, hexokinase and β-galactosidase. However, natural enzymes are expensive due to the complicated separation process and easy denaturation in the surrounding conditions. Thus, many mimetic enzymes have been developed to overcome these disadvantages of natural enzymes. Yan and coworkers first found that Fe_3O_4 nanoparticles have peroxidase-like activity due to their catalytic oxidation of TMB to oxTMB.[1] Subsequently, many nanomaterials such as noble metal nanoparticles,[2–5] metal oxides,[6] metal–organic frameworks[7] also have peroxidase-like activity. This peroxidase-like activity of mimetic enzymes has been used to colorimetrically detect various bio-related substances such as glucose,[8] hydrogen peroxide (H_2O_2),[9] cysteine[10] and glutathione.[11] However, many mimetic enzymes lack stability and biocompatibility in solution, which restrict their accurate detection of bio-related substances in actual tests.[8]

The glucose concentration is closely related to our health and can be detected by using Pd nanoparticles (Pd NPs) based on the colorimetric method. Small Pd NPs have high catalytic capacities due to their enormous specific surface area. However, small Pd NPs are prone to aggregate in solution, which leads to reduced catalytic activity and restricted precision of glucose detection. To address the problem, many synthetic molecules such as PAMAM dendrimers and polyvinylpyrrolidone (PVP) have been developed to stabilize Pd NPs.[12,13] These reagents employed in the preparative process are highly toxic. To avoid the use of toxic materials, green materials such as vitamin C,[14] and green tea extract[15,16] have

[a]State Key Laboratory of Metastable Materials Science and Technology, Yanshan University, Qinhuangdao, 066004, China. E-mail: liangbo@ysu.edu.cn
[b]Key Laboratory of Applied Chemistry, College of Environmental and Chemical Engineering, Yanshan University, Qinhuangdao, 066004, China
[c]Key Laboratory of Biomass Chemical Engineering of Ministry of Education, College of Chemical and Biological Engineering, Zhejiang University, Hangzhou, 310027, China

† Electronic supplementary information (ESI) available. See DOI: 10.1039/d0ra00680g

attracted attention. For example, *Morus nigra* leaf extract and *Asystasia gangetica* leaf extract were used to prepare silver nanoparticles.[17,18] *Euphorbia granulate* extract was used to synthesize Pd NPs in a facile and eco-friendly way in the Suzuki–Miyaura coupling reaction.[19] Barberry fruit extract was used to prepare Pd NPs/RGO by green synthesis to catalyze the reduction of nitroarenes.[20] Many green materials including coffee and tea extract,[21] beet juice,[22] piper longum fruits extract,[23] *Euphorbia thymifolia* L. leaf extract,[24] *Theobroma cacao* L. seeds extract,[25] *Euphorbia neriifolia* L. leaf extract,[26] *Gardenia taitensis* leaf extract,[27] *Solanum melongena* plant extract,[28] *Cucurbita pepo* leaf extract[29,30] have been used to prepare Pd NPs. *Ginkgo biloba* leaf extract was used as a reducing and stabilizing agent to prepare copper nanoparticles,[31] silver nanoparticles[32] and gold nanoparticles.[33] However, *Ginkgo biloba* leaf extract is composed of lactones, flavonoids, polyphenol, acids and polysaccharide.[32] These substances have different reducing power,[34] which may lead to broad size distribution of metal nanoparticles. Flavonoids and polyphenol in the extract are good for the formation of metal nanoparticles.[19] Apart from flavonoids and polyphenol, *Ginkgo biloba* leaf polysaccharide (GBLP) is water-soluble biomacromolecule. The results of scavenging activity of free radical of hydroxyl, DPPH and superoxide radicals demonstrated high antioxidant activities of GBLP.[35] In addition, *Ginkgo biloba* leaf can be obtained easily with low price. It should be suitable for the preparation of highly stable Pd NPs without additional components due to the solubility and antioxidant activity of GBLP.[36]

Herein, Pd_n-GBLP NPs were prepared using GBLP through a green method. The molar ratio of GBLP and Na_2PdCl_4 was used to tune the size of Pd NPs. Pd_{91}-GBLP NPs had good stability and excellent biocompatibility for HeLa cells. They catalyzed oxidation of colorless TMB into blue oxTMB whose absorbance at 652 nm was linear with the glucose concentration. This established method had high sensitivity and selectivity, indicating effective method in bio-related detection. To the best of our knowledge, it is the first time that Pd_n-GBLP NPs were used for colorimetric glucose detection.

2. Results and discussion

2.1 Pd_n-GBLP NPs synthesis and characterization

Ginkgo biloba is an abundantly available and valuable tree plant in China. The leaves of *Ginkgo biloba* have wide medicinal applications in treating illness. GBLP is one of the active components. GBLP and Na_2PdCl_4 were reacted at different molar ratios to obtain Pd_n-GBLP NPs ($n = 41, 68, 91, 137$). This reduction process was monitored by UV-Vis spectra. As shown in Fig. 1a, $PdCl_4^{2-}$ had an obvious characteristic absorption peak at 420 nm. After the incubation of GBLP and Na_2PdCl_4, the peak at 420 nm weakened, indicating the reduction of $PdCl_4^{2-}$ by GBLP. In addition, when the molar ratio of $PdCl_4^{2-}$ to GBLP increased from 41 to 137, Fig. 1b showed absorbance increased. The samples of Pd_n-GBLP NPs were well dissolved in aqueous solution. Taken together, the UV-Vis spectra and solution color demonstrated the successful preparation of Pd_n-GBLP NPs. In this reaction, the reduction of $PdCl_4^{2-}$ was caused by the presence of reducing group such as hydroxyl group and aldehyde group in the GBLP.

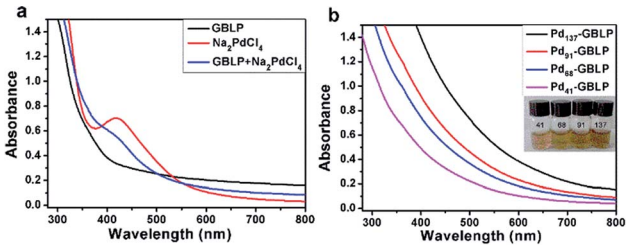

Fig. 1 (a) UV-Vis spectra of GBLP, Na_2PdCl_4, GBLP + Na_2PdCl_4, (b) UV-Vis spectra and photos of 5 μM of Pd_n-GBLP NPs.

The sizes of Pd NPs inside of Pd_n-GBLP NPs were investigated by TEM. Fig. 2 showed Pd NPs are spherical and monodisperse. The calculated average diameter of Pd NPs was 7.61 ± 1.74 nm for Pd_{41}-GBLP; 9.62 ± 2.53 nm for Pd_{68}-GBLP; 11.10 ± 2.76 nm for Pd_{91}-GBLP and 13.13 ± 2.64 nm for Pd_{137}-GBLP,

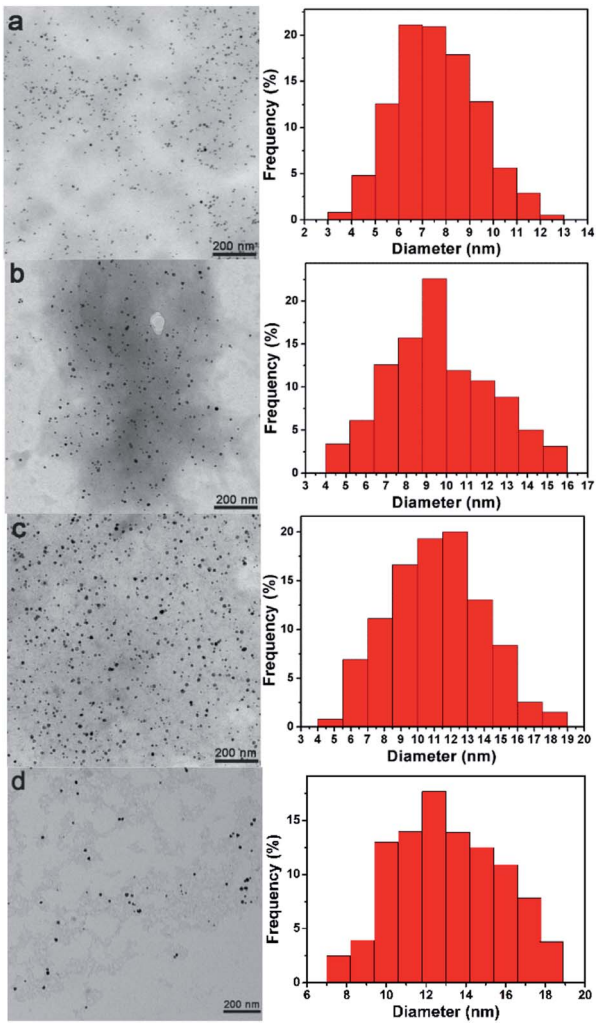

Fig. 2 TEM images and corresponding size distribution histograms of (a) Pd_{41}-GBLP, (b) Pd_{68}-GBLP, (c) Pd_{91}-GBLP and (d) Pd_{137}-GBLP.

respectively. The specific surface area was 0.79 nm^{-1} for Pd_{41}-GBLP; 0.62 nm^{-1} for Pd_{68}-GBLP; 0.54 nm^{-1} for Pd_{91}-GBLP; and 0.46 nm^{-1} for Pd_{137}-GBLP, respectively. In contrast, Dong and coworkers used *Ginkgo biloba* leaf extract to prepare Au NPs with wide size distribution (10–40 nm).[19] This should be due to the complicated composition of *Ginkgo biloba* leaf extract. Compared with this result, Pd NPs inside of Pd_n-GBLP had smaller size (7–13 nm) and narrow size distribution.

The elemental composition and formation of Pd_n-GBLP NPs were further verified by X-ray photoelectron spectroscopy (XPS). Fig. 3a showed the XPS spectrum of Pd_{91}-GBLP NPs. The peaks of C 1s and O 1s were clearly located at 284.6 and 532.76 eV. Both peaks were derived from GBLP, indicating that GBLP played a key role in stabilizing Pd NPs as a template. Fig. 3b was a high-resolution spectrum of Pd NPs with peaks at 336.15 and 341.47 eV corresponding to Pd $3d_{5/2}$ and Pd $3d_{3/2}$, respectively, which was consistent with the previously reported binding energy position of metallic Pd.[37,38] The binding energy of Pd_n-GBLP was slightly different from the bulk materials of Pd because the surface binding energy was dependent on the surface chemical composition and size of nanoparticles.[39] Thus, XPS spectrum results confirmed that zero-valent Pd NPs were successfully prepared by using GBLP as a reducing agent and stabilizer.

The crystal form and spatial structure of Pd NPs synthesized by GBLP were characterized by XRD.[40] As shown in Fig. 4, there were five different reflections at 40.14° (111), 46.58° (200), 68.04° (220), 82.02° (311) and 86.08° (222). These characteristic reflections proved that the Pd NPs in Pd_{91}-GBLP NPs were a face-centered cubic (fcc) structure (JCPDS: 87–0641, space group: *Fm*3*m* (225)). This was the same as shape memory cellulose nanofibril aerogels decorated with Pd NPs prepared by Jin Gu and coworkers[41] and pallet nanoparticles using *Pulicaria glutinosa* extract prepared by Khan and coworkers.[42]

The hydrodynamic size and zeta potential of Pd_n-GBLP NPs were measured using DLS technology. As shown in Fig. 5a, the hydrodynamic size of Pd_{41}-GBLP NPs was 21.4 nm for Pd_{41}-GBLP NPs; 22.1 nm for Pd_{68}-GBLP NPs; 23.1 nm for Pd_{91}-GBLP NPs and 25.9 nm for Pd_{137}-GBLP NPs. The hydrodynamic size of Pd_n-GBLP NPs included GBLP molecule, which was much bigger than the size of Pd NPs measured using TEM. Furthermore, the zeta potential of Pd_n-GBLP NPs was also measured at 7.4. Fig. 5b showed the zeta potential of Pd_n-GBLP NPs were about 0 mV. In addition, the stability of Pd_{91}-GBLP NPs was measured by their

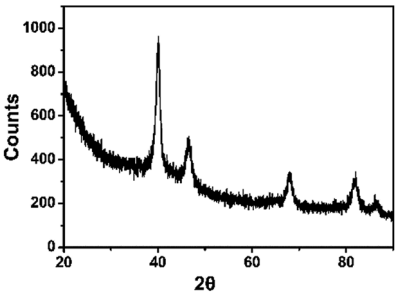

Fig. 4 The XRD pattern of Pd_{91}-GBLP NPs.

hydrodynamic sizes in different buffer. As shown in Fig. 5c, Pd_{91}-GBLP NPs maintained their size about 22 nm within one week, suggesting they had good stability in harsh conditions for a long time. Zeta potential and steric hindrance affect the stability of the nanoparticles in solution.[43,44] Highly charged nanoparticles with zeta potential above 30 mV have good stability. Furthermore, macromolecules are also used to stabilize nanoparticles due to their steric effects.[45] As for Pd_{91}-GBLP NPs, Fig. 5d showed that the zeta potential of Pd_{91}-GBLP NPs was about 0 mV in different pH buffer. Thus, the steric hindrance of GBLP was the main reason for the high stability of Pd_{91}-GBLP NPs. The high stability of Pd_{91}-GBLP NPs was beneficial to high catalytic activity in complex environments for a long time.

2.2 Biocompatibility

Furthermore, the biocompatibility of Pd_{91}-GBLP NPs was evaluated by MTT assay and morphology observation.[46,47] As shown in Fig. 6a, cell viability of HeLa cells was higher than 92.3% when the concentration of Pd_{91}-GBLP NPs was within 0–500 μg mL^{-1}. At 500 μg mL^{-1}, the morphologies of HeLa cells treated with GBLP (Fig. 6c) and Pd_{91}-GBLP NPs (Fig. 6d) were similar to that of control groups (Fig. 6b). The results indicated that Pd_{91}-GBLP NPs had good biocompatibility towards HeLa cells up to

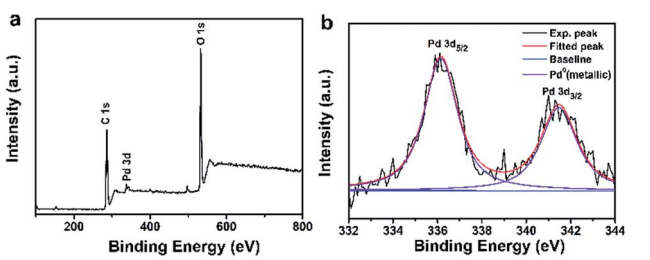

Fig. 3 (a) XPS spectrum of Pd_{91}-GBLP NPs and (b) high-resolution spectrum of the Pd 3d.

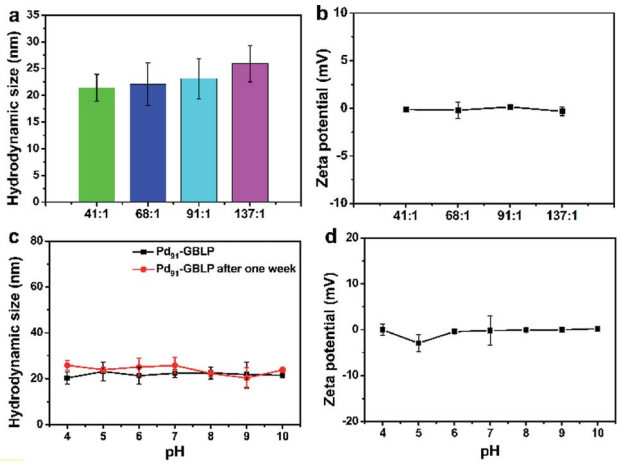

Fig. 5 (a) The hydrodynamic size and (b) zeta potential of Pd_n-GBLP NPs in buffer, (c) the hydrodynamic size and (d) zeta potential of Pd_{91}-GBLP NPs in different pH buffer.

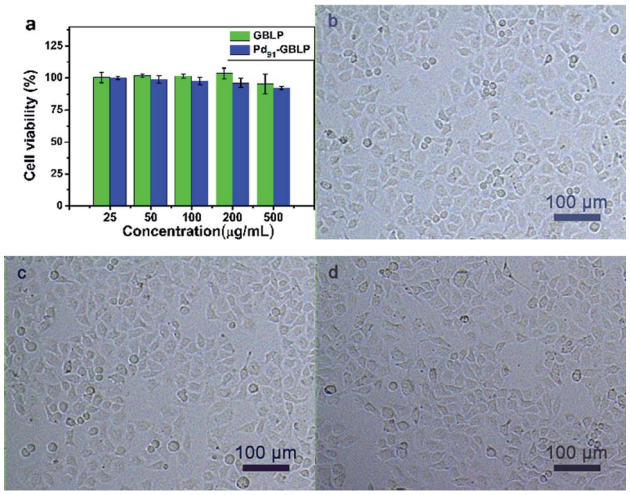

Fig. 6 (a) Cell viability of HeLa cells and photos after HeLa cells incubated with (b) control groups, (c) GBLP and (d) Pd_{91}-GBLP NPs after 24 h.

500 μg mL^{-1}. The presence of biocompatible GBLP should lead to enhanced biocompatibility of Pd_{91}-GBLP NPs. The high biocompatibility of Pd_{91}-GBLP NPs was good for their application in the bio-related medium.

2.3 Peroxidase-like activity of Pd_n-GBLP NPs

In order to study the peroxidase-like activity of Pd_n-GBLP NPs, TMB was used as a chromogenic substrate. As displayed in Fig. 7a, the group [TMB + Pd_{91}-GBLP + H_2O_2] had the highest absorption peak at 652 nm among all samples. In contrast, neither the group [TMB + H_2O_2] nor the group [TMB + Pd_{91}-GBLP] got an obvious absorption band at 652 nm. These results indicated that three components were required and that Pd_{91}-GBLP NPs quickly oxidized the oxidation of TMB with H_2O_2. The group [TMB + Pd_{91}-GBLP + H_2O_2] also produced obvious blue color in Fig. 7b. Thus, Pd_{91}-GBLP NPs catalyzed colorless TMB into a blue oxTMB in the presence of H_2O_2. Pd_{91}-GBLP NPs should facilitate the electron transfer between TMB and H_2O_2. Other nanoparticles such as Pt nanoclusters,[48] rhodium nanoparticles[49] and CeO_2 nanoparticles[50] have been also reported to exhibit peroxidase-like activity.

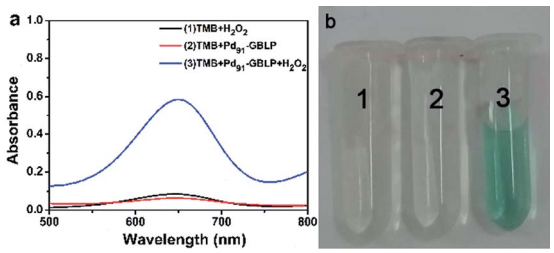

Fig. 7 (a) Typical absorption spectra of the different solutions: [TMB + H_2O_2], [TMB + Pd_{91}-GBLP], [TMB + Pd_{91}-GBLP + H_2O_2] and (b) corresponding solution.

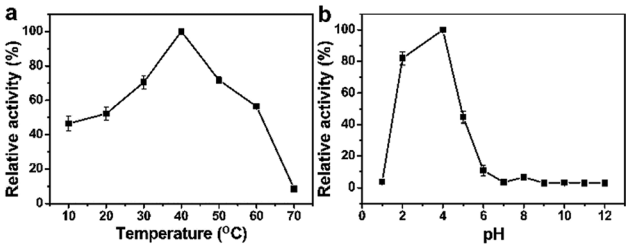

Fig. 8 Effects of (a) temperature and (b) pH on the peroxidase-like property of Pd_{91}-GBLP NPs.

Parameters such as solution temperature and pH had a significant effect on the catalytic activity of the peroxidase mimetic.[51] As shown in Fig. 8a, they had the highest absorbance at 40 °C when the temperature was from 10 to 70 °C. In addition, Fig. 8b showed that Pd_{91}-GBLP NPs exhibited the highest catalytic activity at pH 4 when the pH was from 1 to 12. The optimal condition was related to the stability of H_2O_2. Thus, the optimal conditions were temperature 40 °C and pH 4.0.

2.4 Kinetic and mechanism study

The catalytic behaviors of Pd_{91}-GBLP NPs with H_2O_2 or TMB as substrates were further studied to get the steady-state kinetic parameters. The kinetic experiments were carried out by changing the concentration of TMB or H_2O_2 and fixing the others. As illustrated in Fig. 9a and b, the catalytic steady-state kinetic of Pd_n-GBLP NPs with TMB and H_2O_2 followed the typical Michaelis–Menten curve. As shown in Fig. 9c and d, the effect of the reciprocal substrate concentration on the reciprocal initial velocity was drawn. The parallel lines reflected that their slopes were similar and manifested the ping-pong mechanism

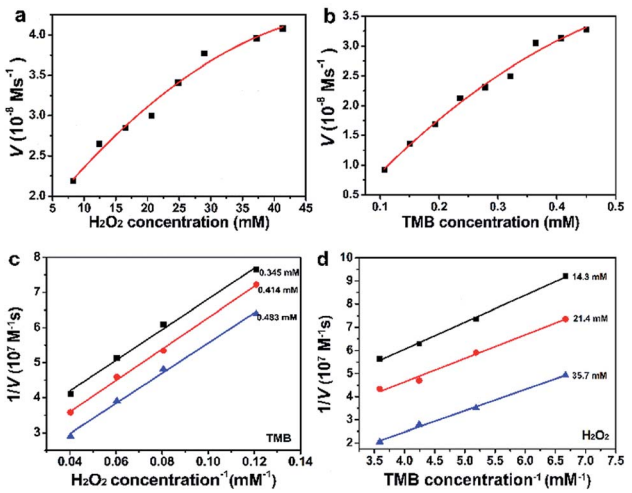

Fig. 9 Steady-state kinetic assay of P_{91}-GBLP NPs. (a) The TMB was 0.414 mM with varying H_2O_2 concentration. (b) The H_2O_2 was 21.4 mM with varying TMB concentration. (c and d) The double reciprocal plots with respect to H_2O_2 or TMB concentration, respectively.

Table 1 Comparison of the kinetic parameters of mimetic enzyme and HRP

Catalyst	Substrate	K_m [mM]	V_{max} [10^{-8} M s^{-1}]	Ref.
Pd_{91}-GBLP	TMB	2.43	22.6	This work
Pd_{91}-GBLP	H_2O_2	10.75	4.93	
HRP	TMB	0.434	10.0	1
HRP	H_2O_2	3.70	8.71	

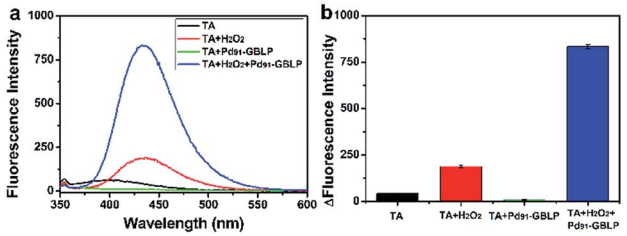

Fig. 10 (a) The fluorescence spectra of [TA + H_2O_2 + Pd_{91}-GBLP NPs] and control groups and (b) histograms of fluorescence intensity.

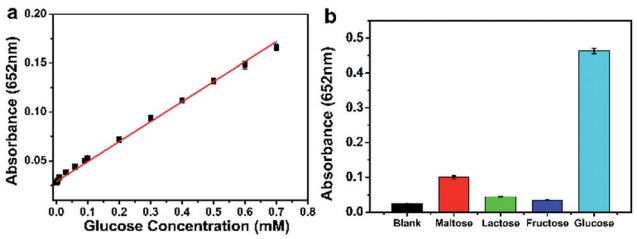

Fig. 11 Glucose detection using Pd_{91}-GBLP NPs. (a) The linear plot in the range of 2.5–700 μM. (b) The absorbance of glucose (5 mM) and other sugars (10 mM).

of catalytic oxidation.[1] The Michaelis–Menten constant (K_m) and maximal reaction velocity (V_{max}) were calculated from Lineweaver–Burk plots and were summarized in Table 1. The K_m of Pd_{91}-GBLP with TMB as substrate was 2.43 mM, the K_m of Pd_{91}-GBLP with H_2O_2 as substrate was 10.75 mM. Both parameters were larger than those of HRP, indicating the lower affinity of Pd_{91}-GBLP than that of HRP. In contrast, the V_{max} (22.6×10^{-8} M s^{-1}) for TMB of Pd_{91}-GBLP was much higher than that (10.0×10^{-8} M s^{-1}) of HRP, indicating Pd_{91}-GBLP had higher catalytic activity for the oxidation of TMB.

To further investigate the catalytic mechanism of Pd_{91}-GBLP NPs as a mimetic enzyme, the role of H_2O_2 in the chromogenic reaction was measured using terephthalic acid (TA). TA can be reacted with hydroxyl radical (HO$^\bullet$) to convert 2-hydroxy terephthalic acid (TAOH) which has the maximal fluorescence peak at 430 nm.[52] As shown in Fig. 10a, the group [TA + H_2O_2 + Pd_{91}-GBLP] had the highest fluorescence intensity in tested samples. The fluorescence intensity of TA, [TA + H_2O_2], [H_2O_2 + Pd_{91}-GBLP] and [TA + H_2O_2 + Pd_{91}-GBLP] was 41.7, 187.8, 9.7 and 834.4, respectively. The results indicated that Pd_{91}-GBLP NPs catalyzed the decomposition of H_2O_2 into HO$^\bullet$ and the HO$^\bullet$ quickly oxidized TMB into blue oxTMB in acidic media. The result was consisted with previous reports. CeO_2-MMT nanocomposites[53] and FeS_2 nanoparticles[11] enhanced the generation of HO$^\bullet$ from the decomposition of H_2O_2.

2.5 Colorimetric glucose detection

Glucose and oxygen can be catalyzed by glucose oxidase (GOD) to produce gluconic acid and H_2O_2. And the concentration of H_2O_2 was linear with the color change of oxTMB in the peroxidase-like reaction of Pd_{91}-GBLP NPs. Therefore, a colorimetric method of glucose detection was designed by detecting the absorbance of oxTMB catalyzed by Pd_{91}-GBLP NPs. Fig. 11a depicted the absorbance of oxTMB was linear with the glucose concentration. The equation of linear regression was $y = 0.20438x + 0.02882$ ($R^2 = 0.995$). The linear range for glucose was from 2.5 to 700 μM. As shown in Table 2, the detection limit was 1 μM which was lower than those of GK-Pd NPs, NiPd hNPs and Fe–Pd/rGO. Thus, Pd_{91}-GBLP NPs had higher sensitivity than other mimetic enzyme in glucose detection. Furthermore, the selectivity of this method was measured. Fig. 11b showed that the absorbance of blank, maltose, lactose, fructose and glucose was 0.025, 0.100, 0.045, 0.035 and 0.463, respectively. Thus, when the glucose concentration was half of other sugars, the absorbance of glucose group was much higher than those of other groups. Thus, other sugars had no interference with the detection of glucose. Human serum was used as a real sample to test the accuracy of this method. The experimental result was 8.42 mM (RSD = 2.6%) and the glucose concentration measured by the hospital was 8.30 mM. Thus, the established method had good accuracy and practical application.

Table 2 Comparison of linear range and detection limit of glucose between Pd_{91}-GBLP and other mimetic enzyme

Mimetic enzyme	Linear range (μM)	Detection limit (μM)	Method	Reference
Pd_{91}-GBLP	2.5–700	1	Colorimetry	This work
GK-Pd NPs	10–1000	6	Colorimetry	54
Cu–Pd/rGO	0.2–50	0.29	Colorimetry	55
NiPd hNPs	5–500	4.2	Colorimetry	56
Fe–Pd/rGO	0–200	1.76	Colorimetry	57
Pd–Ni/SiNW	2000–20 000	2.88	Electrochemistry	58
Pd–Au/GOx/C	50–10 000	1.4	Electrochemistry	59
PtPd/PHNG-2	100–4000	1.82	Electrochemistry	60

3. Conclusion

To summarize, a new green method that GBLP was used to prepare stable and biocompatible Pd_n-GBLP NPs was demonstrated, where GBLP was used as a reducing and stabilizing agent. The sizes of Pd NPs inside of Pd_n-GBLP NPs were from 7.61 to 13.13 nm with narrow size distribution. Pd_n-GBLP NPs had long-term stability in different buffer solutions. Pd_{91}-GBLP NPs were also highly biocompatible with HeLa cells even when the concentration of Pd_{91}-GBLP NPs was 500 μg mL^{-1}. The GBLP resulted in the high stability and biocompatibility of Pd_{91}-GBLP NPs. More importantly, Pd_{91}-GBLP NPs had peroxidase-like properties and typical Michaelis–Menten kinetics. The catalytic reaction followed a ping-pong mechanism. The catalytic reaction by Pd_{91}-GBLP NPs was used to sensitively detect the glucose concentration. This colorimetric method had high selectivity, wide linear range, low detection limit and good accuracy for the detection of glucose concentrations. The enhanced stability and biocompatibility were good for their application. The native resources in the developing countries can be used to produce most of plant-based products by a facile way.

Conflicts of interest

There are no conflicts of interest to declare.

Acknowledgements

The authors appreciate financial support from Natural Science Foundation of Hebei Province (B2017203229) and China Postdoctoral Science Foundation (2016M601284).

Notes and references

1 L. Gao, J. Zhuang, L. Nie, J. Zhang, Y. Zhang, N. Gu, T. Wang, J. Feng, D. Yang, S. Perrett and X. Yan, *Nat. Nanotechnol.*, 2007, **2**, 577–583.
2 W. Zhang, X. Niu, S. Meng, X. Li, Y. He, J. Pan, F. Qiu, H. Zhao and M. Lan, *Sens. Actuators, B*, 2018, **273**, 400–407.
3 H.-H. Deng, X.-L. Lin, Y.-H. Liu, K.-L. Li, Q.-Q. Zhuang, H.-P. Peng, A.-L. Liu, X.-H. Xia and W. Chen, *Nanoscale*, 2017, **9**, 10292–10300.
4 X.-Q. Lin, H.-H. Deng, G.-W. Wu, H.-P. Peng, A.-L. Liu, X.-H. Lin, X.-H. Xia and W. Chen, *Analyst*, 2015, **140**, 5251–5256.
5 Y. Cui, J. Zhang, Q. Yu, X. Guo, S. Chen, H. Sun, S. Liu, L. Wang, X. Lai and D. Gao, *New J. Chem.*, 2019, **43**, 9076–9083.
6 Y. Gao, K. Wu, H. Li, W. Chen, M. Fu, K. Yue, X. Zhu and Q. Liu, *Sens. Actuators, B*, 2018, **273**, 1635–1639.
7 C. Wang, J. Gao, Y. Cao and H. Tan, *Anal. Chim. Acta*, 2018, **1004**, 74–81.
8 X. Liu, D. Huang, C. Lai, L. Qin, G. Zeng, P. Xu, B. Li, H. Yi and M. Zhang, *Small*, 2019, **15**, 1900133.
9 W. Deng, Y. Peng, H. Yang, Y. Tan, M. Ma, Q. Xie and S. Chen, *ACS Appl. Mater. Interfaces*, 2019, **11**, 29072–29077.
10 C. Chen, Y. Wang and D. Zhang, *Microchim. Acta*, 2019, **186**, 784.
11 C. Song, W. Ding, W. Zhao, H. Liu, J. Wang, Y. Yao and C. Yao, *Biosens. Bioelectron.*, 2020, **151**, 111983.
12 C. Deraedt, G. Melaet, W. T. Ralston, R. Ye and G. A. Somorjai, *Nano Lett.*, 2017, **17**, 1853–1862.
13 Y. Li, E. Boone and M. A. El-Sayed, *Langmuir*, 2002, **18**, 4921–4925.
14 V. Smuleac, R. Varma, B. Baruwati, S. Sikdar and D. Bhattacharyya, *ChemSusChem*, 2011, **4**, 1773–1777.
15 V. Smuleac, R. Varma, S. Sikdar and D. Bhattacharyya, *J. Membr. Sci.*, 2011, **379**, 131–137.
16 J. Virkutyte and R. S. Varma, *Chem. Sci.*, 2011, **2**, 837–846.
17 R. A. Hafez, M. A. Abdel-Wahhab, A. F. Sehab and A.-Z. A. K. El-Din, *J. Anim. Plant Sci.*, 2017, **7**, 041–048.
18 A. Jose, T. Abirami, V. Kavitha, R. Sellakilli and J. Karthikeyan, *J. Pharmacogn. Phytochem.*, 2018, **7**, 2453–2457.
19 M. Nasrollahzadeh and S. Mohammad Sajadi, *J. Colloid Interface Sci.*, 2016, **462**, 243–251.
20 M. Nasrollahzadeh, S. Mohammad Sajadi, A. Rostami-Vartooni, M. Alizadeh and M. Bagherzadeh, *J. Colloid Interface Sci.*, 2016, **466**, 360–368.
21 M. N. Nadagouda and R. S. Varma, *Green Chem.*, 2008, **10**, 859–862.
22 J. Kou and R. S. Varma, *RSC Adv.*, 2012, **2**, 10283–10290.
23 A. Hatamifard, M. Nasrollahzadeh and J. Lipkowski, *RSC Adv.*, 2015, **5**, 91372–91381.
24 M. Nasrollahzadeh, S. M. Sajadi, E. Honarmand and M. Maham, *New J. Chem.*, 2015, **39**, 4745–4752.
25 M. Nasrollahzadeh, S. M. Sajadi, A. Rostami-Vartooni and M. Bagherzadeh, *J. Colloid Interface Sci.*, 2015, **448**, 106–113.
26 M. Maryami, M. Nasrollahzadeh, E. mehdipour and S. M. Sajadi, *Sep. Sci. Technol.*, 2017, **184**, 298–307.
27 M. Nasrollahzadeh, S. M. Sajadi, M. Maham and I. Kohsari, *Microporous Mesoporous Mater.*, 2018, **271**, 128–137.
28 M. Nasrollahzadeh, F. Ghorbannezhad and S. M. Sajadi, *Appl. Organomet. Chem.*, 2019, **33**, e4698.
29 M. Nasrollahzadeh, F. Ghorbannezhad, S. M. Sajadi and R. S. Varma, *Nanomaterials*, 2019, **9**, 565.
30 M. Nasrollahzadeh, M. Sajjadi, J. Dadashi and H. Ghafuri, *Adv. Colloid Interface Sci.*, 2020, **276**, 102103.
31 M. Nasrollahzadeh and S. Mohammad Sajadi, *J. Colloid Interface Sci.*, 2015, **457**, 141–147.
32 Y.-y. Ren, H. Yang, T. Wang and C. Wang, *Phys. Lett. A*, 2016, **380**, 3773–3777.
33 J. Zha, C. Dong, X. Wang, X. Zhang, X. Xiao and X. Yang, *Optik*, 2017, **144**, 511–521.
34 T. Wang, R. Jónsdóttir and G. Ólafsdóttir, *Food Chem.*, 2009, **116**, 240–248.
35 B. Jiang, H. Zhang, C. Liu, Y. Wang and S. Fan, *Med. Chem. Res.*, 2010, **19**, 262–270.
36 H. M. El-Rafie, M. H. El-Rafie and M. K. Zahran, *Carbohydr. Polym.*, 2013, **96**, 403–410.
37 H. L. Parker, J. R. Dodson, V. L. Budarin, J. H. Clark and A. J. Hunt, *Green Chem.*, 2015, **17**, 2200–2207.

38 E.-M. Felix, M. Antoni, I. Pause, S. Schaefer, U. Kunz, N. Weidler, F. Muench and W. Ensinger, *Green Chem.*, 2016, **18**, 558–564.
39 X. Fu, Y. Wang, N. Wu, L. Gui and Y. Tang, *J. Colloid Interface Sci.*, 2001, **243**, 326–330.
40 L. Liu, J. Zhang, X. Wang, W. Hou, X. Liu, M. Xu, J. Yang and B. Liang, *Mater. Lett.*, 2020, **258**, 126811.
41 J. Gu, C. Hu, W. Zhang and A. B. Dichiara, *Appl. Catal., B*, 2018, **237**, 482–490.
42 M. Khan, M. Khan, M. Kuniyil, S. F. Adil, A. Al-Warthan, H. Z. Alkhathlan, W. Tremel, M. N. Tahir and M. R. H. Siddiqui, *Dalton Trans.*, 2014, **43**, 9026–9031.
43 L. Wang, X. Zhang, Y. Cui, X. Guo, S. Chen, H. Sun, D. Gao, Q. Yang and J. Kang, *Transit. Met. Chem.*, 2020, **45**, 31–39.
44 X. Zhang, L. Fan, Y. Cui, T. Cui, S. Chen, G. Ma, W. Hou and L. Wang, *Nano*, 2020, **15**(1), 2050002.
45 Y. Zhao, J. Zhang, D. Xie, H. Sun, S. Yu and X. Guo, *J. Biomater. Sci., Polym. Ed.*, 2020, 1–15, DOI: 10.1080/09205063.2020.1716298.
46 L. Wang, L. Zhu, M. T. Bernards, S. Chen, H. Sun, X. Guo, W. Xue, Y. Cui and D. Gao, *ACS Appl. Polym. Mater.*, 2019, DOI: 10.1021/acsapm.9b00026.
47 Y. He, W. Cao, C. Cong, X. Zhang, L. Luo, L. Li, H. Cui and D. Gao, *ACS Sustainable Chem. Eng.*, 2019, **7**, 3584–3592.
48 L. Jin, Z. Meng, Y. Zhang, S. Cai, Z. Zhang, C. Li, L. Shang and Y. Shen, *ACS Appl. Mater. Interfaces*, 2017, **9**, 10027–10033.
49 T. G. Choleva, V. A. Gatselou, G. Z. Tsogas and D. L. Giokas, *Microchim. Acta*, 2017, **185**, 22.
50 B. Jiang, D. Duan, L. Gao, M. Zhou, K. Fan, Y. Tang, J. Xi, Y. Bi, Z. Tong, G. F. Gao, N. Xie, A. Tang, G. Nie, M. Liang and X. Yan, *Nat. Protoc.*, 2018, **13**, 1506–1520.
51 Q. Wang, J. Chen, H. Zhang, W. Wu, Z. Zhang and S. Dong, *Nanoscale*, 2018, **10**, 19140–19146.
52 J. Gao, Q. Li, C. Wang and H. Tan, *Microchim. Acta*, 2017, **185**, 9.
53 L. Sun, Y. Ding, Y. Jiang and Q. Liu, *Sens. Actuators, B*, 2017, **239**, 848–856.
54 L. Rastogi, D. Karunasagar, R. Sashidhar and A. Giri, *Sens. Actuators, B*, 2017, **240**, 1182–1188.
55 G. Darabdhara, P. K. Boruah and M. R. Das, *Microchim. Acta*, 2019, **186**, 13.
56 Q. Wang, L. Zhang, C. Shang, Z. Zhang and S. Dong, *Chem. Commun.*, 2016, **52**, 5410–5413.
57 C. Yang, W. Feng, Y. Li, X. Tian, Z. Zhou, L. Lu and Y. Nie, *Dyes Pigments*, 2019, **164**, 20–26.
58 S. Hui, J. Zhang, X. Chen, H. Xu, D. Ma, Y. Liu and B. Tao, *Sens. Actuators, B*, 2011, **155**, 592–597.
59 H. Celik Kazici and M. Yayla, *Chem. Eng. Commun.*, 2019, 1–12.
60 A. Salah, N. Al-Ansi, S. Adlat, M. Bawa, Y. He, X. Bo and L. Guo, *J. Alloys Compd.*, 2019, **792**, 50–58.

